Photoelectrons in Rb/THF Solution: Spectral Dependence of Photodetachment Cross-Section

V. Rozenshtein, Y. Heimlich, and H. Levanon*

Department of Physical Chemistry and the Farkas Center for Light-Induced Processes, The Hebrew University of Jerusalem

L. Lukin

Institute for Energy Problems in Chemical Physics, Russian Academy of Sciences, Chernogolovka, Moscow Region 142432, Russian Federation

Received: August 24, 2000; In Final Form: January 4, 2001

Photoconductivity method, combined with laser pulse excitation, was employed to obtain the spectral dependence of electron photodetachment in rubidium-tetrahydrofuran (Rb/THF) solution at room temperature. Wavelength dependence of photodetachment cross section, σ_{pd}, qualitatively retraces that of the optical absorption cross section, σ_a. Moreover, a wavelength dependence of the quantum yield, $\kappa = \sigma_{pd}/\sigma_a$, was also found, where $\kappa \approx 0.03$ is held constant for the wavelengths region $\lambda \geq 680$ nm ($h\nu \leq 1.8$ eV). Also, in the short wavelengths region, $\lambda \leq 510$ nm ($h\nu \geq 2.4$ eV), κ is constant, but almost three times larger ($\kappa \approx 0.085$). The inflection region is located approximately at $h\nu = 2.2$ eV, that coincides with the energy of Rb^- ground state relative to the lower edge of the conduction band of THF. Mechanism of Charge-Transfer-To-Solvent (CTTS) with a subsequent release of a solvated electron is suggested to be valid below the conduction band of Rb/THF. It implies that $\kappa = k_s/(k_s + k_c) \approx 0.03$, and consequently, $k_c = 30k_s$, where k_c is the rate constant of the radiationless interconversion, and k_s is the rate constants of the isomerization of CTTS excited state with the formation of the solvated electron. When photon energy becomes higher than the energetic gap between the CTTS ground state and the edge of the THF conduction band, photoinduced autoionization transitions into the continuum generate quasi-free electrons.

I. Introduction

Photodetachment is the photoionization of a negative ion, where the final state is a neutral atom (or molecule) and an electron. Atomic negative ions in a vacuum normally have only one bound state (i.e., the ground state) and, thus, the absorption spectra of such anions are expected to consist of pure continuum, starting from a frequency corresponding to the binding energy of the anion ground state.[1] The continuum may be structured by the presence of resonance autoionization transitions involving absorption to unstable excited states.[1−3] Contrary to vacuum conditions, in liquid solutions the solvent molecules stabilize the bound excited states of the ion, yielding a strong absorption band in the ultraviolet and visible wavelength regions. This electronic absorption spectrum is the fingerprint of the charge transfer to solvent (CTTS) for which an electron remains attached to the parent atom.[4−14]

In recent years, study of photodetachment in both the gas and fluid phases has become a "hot" subject.[14,15] State-of-the-art optical methods allow photoexcitation and detection on a femtosecond time scale and study of fast dynamics associated with the decay of the anions in their excited states accompanied by the generation of the solvated electron.[13,14] Particularly, it has been shown that just a few neutral molecules (3 to 6) of the "solvent" network (cluster), with an overall dipole moment of 2 D, can bind an electron in a "dipole-bound" state.[14] The latter represents the anion analogue of a Rydberg state, in which the orbital for the excess electron is exceptionally diffusive. For anions, the light-induced transitions from the localized ground-state orbital to the dipole-bound state result in a broad absorption band. As the number of the "solvent" molecules in the cluster increases, this band shifts toward the energy of the CTTS band in solution.[11,14] Thus, a CTTS excited state represents a dipole-bound excited state in solution. The CTTS state with the diffuse electron cloud can be isomerized to different conformers in which the excess electron is more localized. The prevailing number of investigations, devoted to photodetachment, relates to the study of halide (mainly iodide) anions in water, bulk and clusters.[7−14,16]

The purpose of the present study is to gain new insights in photodetachment of a different class of ions, namely alkali metal anions. Photodetachment spectra of the alkali metal anions have not been studied yet, although their CTTS spectra have been obtained and characterized.[6,17−21] In this work, we present a study of electron-transfer processes triggered by the photoexcitation of rubidium anions, Rb^-, dissolved in tetrahydrofuran (Rb/THF). A conductivity method was employed to detect the photodetached excess electrons. It is an extension of our previous work, where we have studied Rb/THF solutions, photoexcited at 532 nm only.[22]

Interestingly, basic photodetachment studies are currently directed toward applied research. For example, shaping the Rydberg or Rydberg-like state wave functions by the laser pulses is associated with application of quantum computers.[15] Second, because in some cases the photodetached electrons are spin-polarized and can be injected into a metal or semiconductor, their transfer through interfaces might be a basis for developing

10.1021/jp003077i CCC: $20.00
Published on Web 03/22/2001

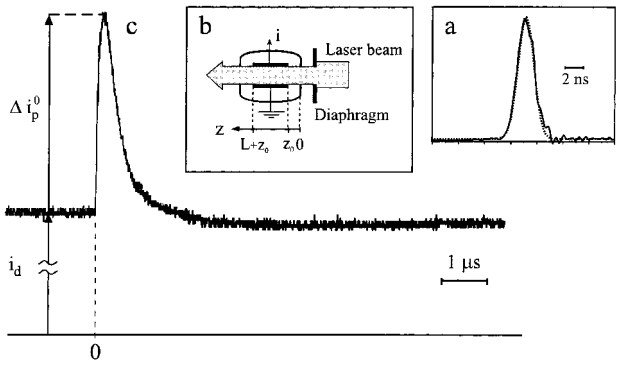

Figure 1. (a) Temporal profile of the laser pulse (solid line) and its simulation (dashed line) based on Gaussian line shape ($\tau_p = 2.2$ ns in eq 12), $\lambda = 475$ nm; (b) Schematic configuration of the photoconductivity cell; (c) An experimental photocurrent trace (the parameters are described in the text).

devices of spin electronics.[23,24] Third, the solvated electrons generated in alkali metal solutions are used in "solvated electron technology" where electrons, as the most powerful reducing agents, destroy toxic wastes.[25]

II. Experimental Section

Photoelectroconductivity measurements were carried out over a wide spectral range (425−1064 nm) and a wide range of pulse energies (0.05−15 mJ). A dye laser (Continuum TDL-60) pumped by a Nd:YAG laser (Continuum YG661 or Continuum Surelite) operating in single shot mode was used. The time profile of the laser pulses and its simulation, based on a Gaussian line shape function, are shown in Figure 1a. The geometry of the cell is shown in Figure 1b. The photoconductivity cell (Pyrex) contained three flat electrodes made of a platinum foil: (1) the collector electrode (length $L = 0.9$ cm, width $b = 0.3$ cm); (2) the high voltage electrode; and (3) the ground electrode, to reduce the dark current signal. The distance between the high voltage and collector electrodes is d (= 0.3 cm). The geometrical area of the collector electrode is A ($= L \times b = 0.27$ cm^2). The laser beam was directed along the long side of the collector electrode and was confined by a 0.3×0.3 cm^2 diaphragm. The light energy, W, of the laser pulse was measured by a phototube (RCA I P39) calibrated with a laser energy meter (Ophir DGX-PP).

To escape irreversible changes in the Rb/THF solution occurring under constant electric field, a voltage pulse (duration of a few ms) synchronized with the laser pulse was applied to the high voltage electrode. The electric field strength, E_0, in the illuminated space was constant and equal to 1.7×10^3 V/cm. Subsequent dark and photoinduced currents were measured as a function of time and laser pulse energy. The response time of the electric circuit was about 20 ns for a load resistor of 200 Ohm.

The observed photodetachment spectrum was compared with the absorption spectrum of the same solution obtained in a quartz cell (1 cm path) with a UV−Vis-IR spectrometer (Shimadzu UV-3101PC). The experiments were carried out at room temperature using solutions with concentrations of the Rb^- ions of $\sim 10^{15}$ cm^{-3}. Rb/THF solutions were prepared by metal dissolution, that is, $2Rb_{solid} \rightleftarrows Rb^- + Rb^+$, carried out by a contact of the solvent with the Rb mirror. Concentrations were measured by absorption spectroscopy and from the dark current, as discussed below. Details of the experimental setup, sample preparation and measurement of currents are described elsewhere.[22]

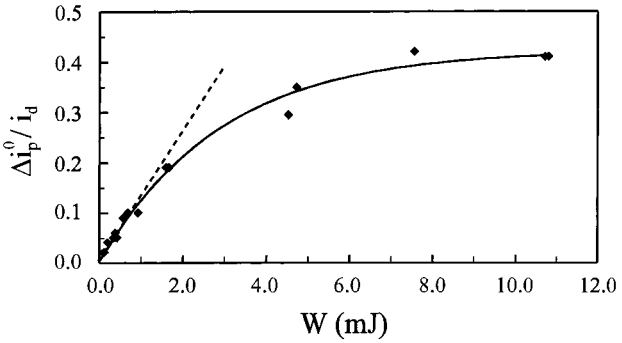

Figure 2. Experimental dependence of the ratio between photoinduced and dark currents, $\Delta i_p^0/i_d$, vs the laser pulse energy, W; $\lambda = 700$ nm.

III. Results and Discussion

1. Experimental Results. Electron photodetachment from Rb^- is described phenomenologically as

$$Rb^- + h\nu \xrightarrow{\sigma_{pd}} Rb\cdot + e_s^- \qquad (1)$$

where Rb· is the neutral atom, e_s^- is the solvated electron, and σ_{pd} is the photodetachment cross section. Typical experimental traces of the dark and photoinduced currents, i_d and Δi_p, respectively, are presented in Figure 1c. Because an electron is much more mobile than Rb^-, the observed photocurrent is mainly attributed to the electrons photodetached from Rb^-. From our earlier results,[22] the initial photocurrent peak, Δi_p^0, and i_d can be expressed as

$$\Delta i_p^0 = e_0 E_0 (\mu_e - \mu_-) A N_e \qquad (2)$$

$$i_d = e_0 E_0 (\mu_+ + \mu_-) A_{eff} (N_1)_0 \qquad (3)$$

where e_0 is the electron charge; E_0 is the electric field applied between the electrodes; A_{eff} is the effective area of the collector electrode ($A/A_{eff} = 0.37$); N_e is the concentration of the solvated electrons; $(N_1)_0$ is the initial concentration of Rb^-; and μ_e, μ_-, and μ_+ are the mobilities of e_s^-, Rb^- and Rb^+, equal to 4.3, 0.8, and 0.8×10^{-3} cm^{2}V^{-1}s^{-1}, respectively. The photocurrent, Δi_p, was found to decay with two characteristic times, a fast one with a few hundred ns followed by a slower decay of tens μs. The photocurrent kinetic traces in the time interval between 100 ns and 1 ms have been carefully analyzed, finding that the decay of the photocurrent to the equilibrium dark current level is caused by secondary electron−ion reactions including a recombination of the photoelectrons with Rb· and Rb^+.[22]

In the present work, we are interested only in the initial photocurrent value, Δi_p^0, and the equilibrium dark current, i_d, because their ratio $\Delta i_p^0/i_d$ carries information on the electron photodetachment cross section.[22] A typical dependence of $\Delta i_p^0/i_d$ versus the laser pulse energy, W, is plotted in Figure 2. For each wavelength, $\Delta i_p^0/i_d$ increases linearly only at low pulse energies, $W < 0.3-0.5$ mJ, whereas at higher energies of 10 mJ, the photocurrent is saturated. A similar saturation effect was reported for the electron photodetachment from organic anions in nonpolar liquids.[26−28] Such a behavior was attributed to anion depletion during the laser pulse.

The experimental CTTS optical spectrum of Rb^- dissolved in THF, in terms of the photon energy (E_p) and the absorption cross section (σ_a) is shown in Figure 3 (solid curve) and agrees well with previous data.[6,17−20] Analogous to the method used in previous studies,[18,29] the spectrum was fitted by combining together Gaussian and Lorentzian shape functions with a

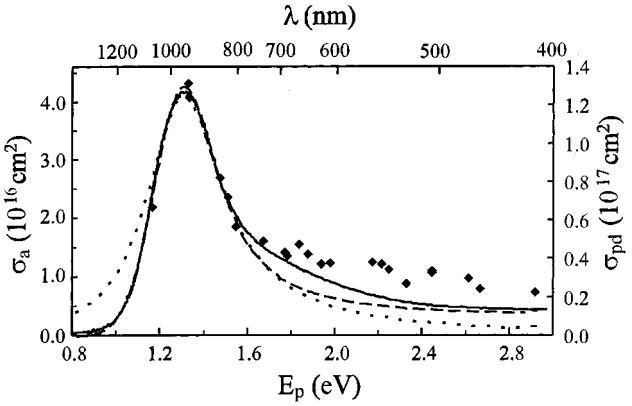

Figure 3. (a) Solid: Experimental absorption cross section of Rb^-, σ_a, as a function of wavelength (left scale); (b) Dashed: Simulation of the absorption spectrum of Rb^- by a Gaussian line shape for $E_p < E_{p,max}$ and a Lorentzian line shape for $E_p > E_{p,max}$; (c) Diamonds: Experimental wavelength dependence of the photodetachment cross section, σ_{pd}, of Rb^- (right scale); (d) Dotted: Simulation of the absorption spectrum of Rb^- by homogeneously broadened line shape (eq 4).

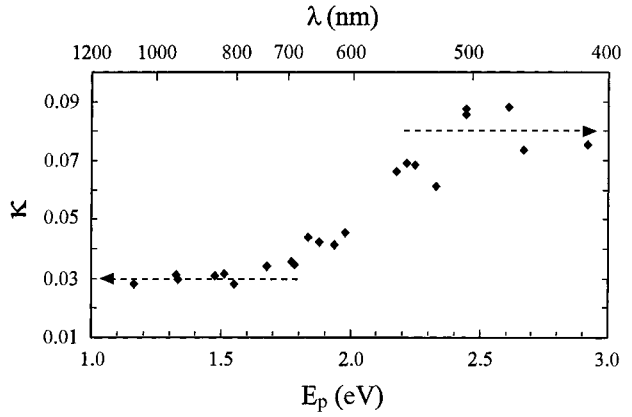

Figure 4. Quantum yield of the solvated electrons, κ, vs photon energy, E_p.

common maximum at 10 640 cm^{-1} (940 nm) and the corresponding portions of the half-width $\Delta\nu^G_{1/2} = 1640$ cm^{-1} and $\Delta\nu^L_{1/2} = 1760$ cm^{-1} for the long (Gaussian) and short (Lorentzian) wavelength regions, respectively (dashed curve, Figure 3). The extinction coefficient, $\epsilon_{max}(Rb^-)$, was found to be $1.0 \pm 0.1 \times 10^5$ M^{-1} cm^{-1} in line with previous data.[18] The formal oscillator strength of Rb^- absorption band, $f = 1.94$, was calculated using the expression: $f = 4.3 \times 10^{-9}\ \epsilon_{max}\ (1.065\ \Delta\nu^G_{1/2} + 1.571\ \Delta\nu^L_{1/2})$.[29] The calculated f value is almost twice as large as that for one-electron totally allowed transition. This implies that the line shape has to be attributed to a superposition of several transitions. The nature of these transitions will be discussed below.

In the experiments, we could not detect the spectrum of the solvated electron e_s^- ($\epsilon_{max} = 4 \times 10^4$ M^{-1} cm^{-1} at the maximum of 2100 nm), nor that of the ion pair (Rb^+, e_s^-) ($\epsilon_{max} = 2 \times 10^4$ M^{-1} cm^{-1} at the maximum of 1200 nm).[17,30] These observations are in line with our studies showing that in Rb/THF under equilibrium conditions (no light or low-intensity light), $[Rb^-] \gg [e_s^-]$, $[Rb^+, e_s^-]$, that is, the processes $Rb^- \rightleftarrows Rb\cdot + e_s^-$ and $Rb^+ + e_s^- \rightleftarrows (Rb^+, e_s^-)$ are insignificant.[22]

The experimental values of σ_{pd} and the quantum yield of the photodetachment, $\kappa = \sigma_{pd}/\sigma_a$, are presented in Table 1 (cf. also Figures 3 and 4). It is evident that the spectral shapes of σ_{pd} and σ_a follow each other. However, the absolute values of the photodetachment and absorption cross sections differ by more than an order of magnitude. As to the quantum yield, κ, it exhibits an "s-shape" dependence upon the wavelengths, and it is enhanced upon increase of the photon energy (cf. Figure 4). Expressions to obtain σ_{pd} values from the experimental current traces and the mechanisms leading to photodetachment will be discussed below.

TABLE 1: Experimental Values of the Absorption (σ_a) and Photodetachment (σ_{pd}) Cross Sections

λ nm	$h\nu$ eV	σ_a 10^{-16}, cm^2	σ_{pd} 10^{-16}, cm^2	σ_{pd}/σ_a
425	2.918	0.295	0.022	0.075
465	2.668	0.327	0.024	0.073
475	2.612	0.339	0.030	0.088
506	2.447	0.383	0.033	0.087
507	2.447	0.383	0.033	0.085
532	2.330	0.440	0.027	0.061
552	2.248	0.501	0.034	0.068
560	2.214	0.534	0.037	0.069
570	2.176	0.571	0.038	0.066
627	1.978	0.829	0.038	0.045
640	1.938	0.898	0.037	0.041
660	1.879	0.992	0.042	0.042
675	1.837	1.080	0.047	0.044
695	1.784	1.187	0.041	0.035
700	1.772	1.212	0.043	0.035
737	1.676	1.440	0.049	0.034
800	1.550	2.010	0.056	0.028
820	1.512	2.290	0.072	0.031
840	1.476	2.660	0.082	0.031
930	1.333	4.180	0.124	0.030
934	1.327	4.200	0.131	0.031
1064	1.165	2.370	0.067	0.028

2. Energetics and Charge-Transfer To Solvent. It is well established that a photoexcited electronic state cannot be regarded as simply a "hot" modification of the same molecule in its ground state. In fact, such an electronically excited-state represents a new species with a different electron distribution and bond structure.[31] An important example is the optical transitions between the CTTS ground and excited states.[4−14] The effective length (l_e) associated with the optical transition can be estimated through the expression:[32] l_e (Å) $= (f\ \lambda_{max}/1080)^{1/2}$, where λ_{max} (Å) is the wavelength at the absorption maximum. In the case of Rb/THF, $f \approx 1.94$ and $\lambda_{max} \approx 9400$ Å, and thus, $l_e \approx 4$ Å, which is sufficiently large to imply that the solvent molecules of the first solvation shell are involved in the transition. In fact, very early studies demonstrated that the temperature and solvent dependence of the absorption band in alkali-metal/ether solutions are characteristic of the CTTS transition of the alkali metal anion.[6]

In this section, we shall use a few approaches to calculate energies of the CTTS states. In a simplified approach, the CTTS spectra are interpreted within the framework of the Landau expression for the potential formed due to a dipolar medium:[33] $V(r) = -e_oZ_{eff}/r$ where e_o is the electron charge, $Z_{eff} = (1/n^2 - 1/D)$ is the effective charge number, n is the refractive index, and D is the dielectric constant of the medium. This potential is formed around a negatively charged ion, giving rise to a discrete set of energy levels, E_k, relative to the conduction band of the solvent (Figure 5a), namely $E_k = -m_0e_0^4\ Z_{eff}^2/2\hbar^2k^2$ where m_0 is the electron mass, and k is the integer. For THF, $n = 1.405$ and $D = 7.58$,[34] and thus, the energy E_1 of the ground state is -1.92 eV, and the energy E_2 of the first excited state is -0.48 eV. The difference ($E_2 - E_1$) is the CTTS transition energy for maximum absorption, that is., $h\nu^{CTTS}_{max} \approx 1.4$ eV compared to the experimental value of 1.3 eV.[35]

In a different approach, the energy of the ground state of the anion in a liquid relative to the vacuum level (taken as zero

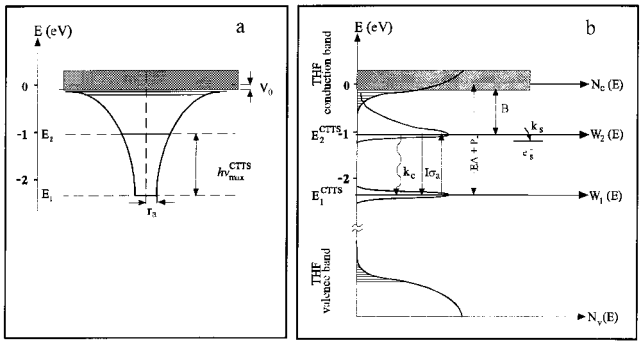

Figure 5. (a) CTTS energy states of Rb^- in the potential created by surrounding solvent THF molecules; (b) Energy scheme of Rb/THF system. All the parameters are described in the text.

energy), E_1^{CTTS}, can be estimated as a sum of the gas-phase electron affinity of an atom EA (= −0.49 eV for Rb) [38] and the polarization energy, P_-,[39,40] that is, $E_1^{CTTS} = EA + P_-$. This polarization energy is the difference between the solvation energies of the anion and the parent atom. According to Born's formula:[39] $P_- = -(e_0^2/2r_a)(1 - 1/D)$, where r_a is the radius of the anionic cavity, which can be calculated from the sum of the radii in a bond between two atoms, independent of the bond's nature, that is, ionic, covalent, or metallic.[41] Thus, $r_a + r_c = 2r_{Rb}$, where r_c (= 1.5 Å) is the radius of Rb^+,[42] and $2r_{Rb}$ = 4.9 Å is the bond length in the metal.[41] As a result, we obtain that r_a = 3.4 Å, P_- = −1.85 eV and E_1^{CTTS} = −2.35 eV (cf. Figure 5b). The calculation of the CTTS energy levels is based on the complete dissociation of the ion pair (Rb^+, Rb^-) in Rb/THF implying that the Coulombic term, due to the ion-pair formation, may by neglected.[22] To calculate E_2^{CTTS} and the energy edge of the conduction band V_0, we shall adopt the approach of Stein and Treinin.[5] On the basis of the Landau's dipolar medium model, they obtained that $E_1^{CTTS} = -h\nu_{max}^{CTTS} - B - V_0$, where the binding energy of the electron in the CTTS excited state is $B = E_2 + P_e$ (cf. Figure 5). In their treatment, E_2 is the Landau's value of the excited-state energy, whereas the electron polarization induced by the excited electron, P_e, obeys the equation: $P_e = (e_0^2/2r_e)(1-1/n^2)$ where r_e (= $6\hbar^2/m_0e_0^2Z_{eff}$) is the mean distance of the excited electron from the anion-cavity center.[5,43] Applying the above expressions to Rb/THF system, B is calculated to be 0.9 eV. Comparison of E_1^{CTTS} = −2.35 eV obtained in the Born's model with the Stein−Treinin expression gives the depth of the THF conduction band V_0 = 0.15 eV (employing the experimental value of $h\nu^{CTTS}{}_{max}$ = 1.3 eV), which is consistent with that obtained elsewhere (V_0 = 0.5 ± 0.5 eV).[29] Finally, in terms of Figure 5b E_2^{CTTS} is calculated to be $B + V_0$ = −1.05 eV.

3. Light Absorption by Rb/THF. In Figure 5b, we present the energy scheme of Rb/THF solution, where the population distributions over the energy levels and kinetic parameters are indicated. The parabolic shape of the valence and conduction bands of THF with the density of states $N_v(E)$ and $N_c(E)$ are shown together with the nonparabolic tails near the edges of the bands.[24,44] The nonparabolic tails are associated with the Anderson's localized states (shown as discrete levels in Figure 5b).[45]

On the basis of Figure 5b, we conclude that light absorption can occur either via the bound−bound transitions between the ground $CTTS_1$ and the excited $CTTS_2$ states (E_p < 2.2 eV) or via the bound-continuum transitions from the $CTTS_1$ state to the conduction band of the solvent (E_p > 2.2 eV). Asymmetry and large spectral width of the optical spectra of halide and alkali metal anions are still poorly understood. On the other hand, the spectroscopy of the simplest anion, the solvated electron, which spectral shape is very similar to that of alkali metal anions, are understood much better.[46−48] For example, it was believed that the optical spectrum of e_s^- is due to the transitions from the s-like ground state to p-like excited states.[49] Both the ground and excited states of e_s^- exist due to the stabilizing potential created by the surrounding solvent molecules (similar to that of Rb^- shown in Figure 5a) and qualitatively described by the Landau's theory of polarons.[33,50] In the computer simulations, the absorption contour of e_s^- was calculated as a superposition of the contributions from three s−p transitions with energy splitting of 0.4 eV between two adjacent s−p transitions.[51] Each transition was taken as inhomogeneously broadened by various structures of the solvent shell. In a recent study, Wiersma and co-workers discovered that the pure dephasing time of the hydrated electron was extremely short (1.6 fs), allowing to describe the complete spectrum by a single homogeneously broadened line.[48,52] If we apply the above findings to the CTTS transitions, then we can try to describe the Rb^- absorption spectrum also as a single homogeneously broadened line, that is[48,52]

$$\sigma_a = \sigma_a^{max}\{4E_p^2(\hbar/T_2)^2/[(E_{p,max}^2 - E_p^2)^2 + 4E_p^2(\hbar/T_2)^2]\} \quad (4)$$

where σ_a^{max} is the maximum value of σ_a at $E_p = E_{p,max}$ and T_2 is the dephasing time of the excited CTTS state. Best fit of σ_a versus E_p with T_2 = 2.85 fs, is shown in Figure 3 (dotted line). It reproduces with the single parameter (T_2) the experimentally obtained spectrum fairly good for its central part, thus, indicating significant contribution of a homogeneous broadening to the line shape. The deviation of the calculated homogeneously broadened spectrum from the experimental one, at low and high photon energies, may be attributed to the influence of the broadening due to the temporal fluctuations of the anionic cavity radius. Contribution of the transitions to the Anderson's states and to the continuum may also account for the quasi-Lorentzian shape of the short-wavelength part of the absorption spectrum (cf. Figure 3). Thus, the wavelength dependence of the absorption cross section (Figure 3) reflects contribution from several electronic transitions of different nature. The fairly good fit obtained by employing a combined Gaussian−Lorentzian line shape function, is a consequence of multiple electronic transitions. The effective oscillator strength of approximately 2 also confirms the inhomogeneous character of the Rb^- absorption. In the case of solvated electrons, a value of $f \approx 1$ was found in a number of liquids,[29] lending support for a single homogeneously broadened line.[48]

The energy distributions over the CTTS states are shown in Figure 5b. The relatively narrow Gaussian energy distribution over the Rb^- ground state ($CTTS_1$) is

$$W_1(E) = (4\pi\lambda_r kT)^{-1/2}\exp[-(E_1^{CTTS} - E)^2/4\lambda_r kT] \quad (5)$$

where $\lambda_r = (e_0^2/2r_a)(1/n^2 - 1/D)$ is the reorganization energy.[53−55] It is due to the distribution of the radii of anionic cavities bound by the solvent molecules and reflects the temporal fluctuations of the electronic level of Rb^-. The CTTS excited state is presented with the broad energy distribution $W_2(E)$, which retraces the spectral line in Figure 3 (dotted curve).

In principle, an electron can be formed either via transition to the CTTS excited state or via photodetachment into the conduction band of the solvent, where the electron is in quasi-free state. In both cases, the initially delocalized electron becomes localized in the solvation shell. In Figure 5b, the energy

of the solvated electron, e_s^-, is shown schematically and can be estimated. The ground-state energy of a solvated electron in THF, E_e, should lie between -0.6 and -3 eV. The former complies with the maximum of the electron absorption spectrum (2100 nm),[17,30] whereas the latter is the energy of hydrated electron.[56] The value of E_e should be higher in THF than in aqua solutions because the ground-state energy of e^-_s increases upon decreasing the polarity.[57,58] Applying the theoretical treatment of Rips and Tachiya,[57,59] the ground-state energy of e_s^- is calculated to be $E_e \approx -1.0$ eV, which puts the energy level of the solvated electron close to that of $CTTS_2$.

4. Photodetachment of Rb^-. On the basis of the CTTS processes within the energy scheme of Figure 5b, we shall develop a model to interpret experimental results (cf. Figure 2). By analogy with the studies of halide aqua solutions, the following reactions in Rb/THF should be taken into account[10,13]

$$Rb^- (CTTS_1) \underset{k_c}{\overset{\sigma_a}{\rightleftharpoons}} Rb^- (CTTS_2) \tag{6}$$

$$Rb^- (CTTS_2) \xrightarrow{k_s} e_s^- + Rb\cdot \tag{7}$$

where $Rb^- (CTTS_1)$ and $Rb^- (CTTS_2)$ are the anion in its CTTS ground and excited states respectively; k_c is the rate constant of the radiationless interconversion; and k_s is the rate constant of the formation of the solvated electron. Processes 6 and 7 are schematically shown in Figure 5b. To a first approximation, we may assume that the rate constant values obtained for the halide aqua solutions,[10,13] that is, $k_c = 5 \times 10^{12}$ s^{-1} and $k_s = 1-2 \times 10^{12}$ s^{-1}, are also valid for Rb/THF (at least, in order of magnitude). In the case of k_c, it can also be estimated from the analogy with the relaxation of the excited state of the hydrated electron.[60−62] In this case, energy is lost via an electronically nonadiabatic p-to-s interconversion transitions with the rate constant of 10^{12} s^{-1} close to k_c obtained for the halide solutions.[63]

The fast reactions 6 and 7 generate the solvated electrons as manifested by the initial photocurrent, Δi_p^0 (cf. Figure 1c). The photocurrent traces following this initial stage, in the micro- and milli-second ranges, are attributed to the reactions $Rb^- \rightleftarrows Rb\cdot + e_s^-$, $Rb\cdot \rightleftarrows Rb^+ + e_s^-$ and $Rb\cdot + Rb\cdot \rightleftarrows Rb^+ + Rb^-$ and were discussed in details elsewhere.[22]

Taking into account processes 6 and 7 and Figure 5b, the following differential equations are associated with the laser pulse absorption in Rb/THF[64]

$$\frac{\partial I}{\partial z} + \frac{1}{c}\frac{\partial I}{\partial t} = -I\sigma_a (N_1 - N_2) \tag{8}$$

$$\frac{\partial N_1}{\partial t} = -I\sigma_a (N_1 - N_2) + k_c N_2 \tag{9}$$

$$\frac{\partial N_2}{\partial t} = I\sigma_a (N_1 - N_2) - k_c N_2 - k_s N_2 \tag{10}$$

where $I \equiv I(z,t)$ is the number of photons passing through a unit cross section of the laser beam per unit time; $N_1 \equiv N_1(z,t)$ and $N_2 \equiv N_2(z,t)$ are the populations of the CTTS ground and excited states respectively; z is the coordinate along the laser beam; and c is the light velocity in THF. Employing a quasi-stationarity principle for the excited state ($\partial N_2/\partial t = 0$), we obtain

$$N_2 = \frac{I\sigma_a}{I\sigma_a + k_s + k_c} N_1 \tag{11}$$

To solve eqs 8, 9, and 11, we transform the coordinate system (t, z) to (τ, ξ), where $\tau = t - z/c$ and $\xi = z$.[65] In terms of the variable τ, the initial laser pulse shape is expressed by a Gaussian function

$$I_0(\tau) = I_m^0 \exp\left[-\frac{\tau}{\tau_p}\right]^2 \tag{12}$$

which fits the experimental pulse with $\tau_p = 2.2$ ns (cf. Figure 1a). In principle, the initial temporal profile of the laser pulse is not retained during the course of its interaction with the absorbing medium. Passing every layer through the sample, the front part of the pulse is absorbed via a spectroscopic transition, whereas later in time the back part of the same pulse causes a light induced emission, thus, restoring the energy absorbed by the medium back to the radiation field.[66] As a consequence, the energy is distributed between two energy reservoirs, the medium and the radiation field. However, when the relaxation rate constants are larger than the rate constant of the light induced emission ($I\sigma_a$), the entering pulse shape is conserved during the light propagation along the sample.[67] This is the case in our system, because k_s, $k_c \gg I\sigma_a$ for $W < 20$ mJ, and thus, the laser pulse shape becomes

$$I(\tau,\xi) = I_m (\xi) \exp\left[-\frac{\tau}{\tau_p}\right]^2 \tag{13}$$

For higher energies, for example, $W > 100$ mJ, eq 13 is invalid.

For a Gaussian shape, the initial energy of the laser pulse is $W = \Phi_0 E_p S = \sqrt{\pi}\, I_m^0\, \tau_p E_p S$, where Φ_0 is the number of photons passing through a unit area; and S is the cross section area of the laser beam. In the present experiments, $W = 0.05-15$ mJ; $E_p = (1.87-4.67) \times 10^{-19}$ J; $I_m^0 = 2.7 \times 10^{23} - 2 \times 10^{26}$ cm^{-2}s^{-1}; and $\tau_p = 2.2$ ns. Typically, experiments are characterized by the low-intensity light pulses, $W < 0.5$ mJ or $I_m^0 < 4 \times 10^{24}$ cm^{-2}s^{-1}. The absorption cross section (cf. Figure 3 and Table 1) and the equilibrium concentration $[Rb^-]_0$ $(= (N_1)_0 \approx 10^{15}$ cm$^{-3})$ were found from the absorption spectrum and the dark current.

In the new coordinate system, eqs 8 and 9 are transformed into[68]

$$\frac{\partial I(\tau,\xi)}{\partial \xi} = -\sigma_a I(\tau,\xi)[N_1(\tau,\xi) - N_2(\tau,\xi)] \tag{14}$$

$$\frac{\partial N_1(\tau,\xi)}{\partial \tau} = -\sigma_a I(\tau,\xi)[N_1(\tau,\xi) - N_2(\tau,\xi)] + k_c N_2(\tau,\xi) \tag{15}$$

For k_s, $k_c \gg I\sigma_a$, the population difference $(N_1 - N_2) \approx N_1$ (eq 11) and with the constraint of eq 13, eq 15 can be solved as

$$N_1 = (N_1)_0 \exp\left\{-\sigma_a \kappa I_m(\xi) \int_{-\infty}^{+\infty} \exp\left[-\frac{\tau}{\tau_p}\right]^2 d\tau\right\} = (N_1)_0 \exp\{-\sqrt{\pi}\,\kappa\sigma_a I_m(\xi)\tau\} \tag{16}$$

where $\kappa = k_s/(k_s + k_c)$ represents the quantum yield of photodetachment. Substituting eq 16 in eq 14 and taking into account the relationship $\sqrt{\pi}\,\kappa\sigma_a\,\tau_p\, I_m^0 \ll 1$ we obtain

$$\frac{\partial I_m(\xi)}{\partial \xi} = -\alpha I_m(\xi) \exp[-\beta I_m(\xi)] \approx -\alpha I(\xi)[1 - \beta I_m(\xi)] \tag{17}$$

where $\alpha = \sigma_a (N_1)_0$ and $\beta = \sqrt{\pi}\,\kappa\sigma_a\tau_p$. The solution of eq 17

for $\sigma_a(N_1)_0 \ll 1$ in the laboratory frame of reference is

$$I_m(z) = \frac{I_m^0}{(1-\alpha\beta z I_m^0)}\exp(-\alpha z) \tag{18}$$

which reduces into Beer−Lambert law for $\alpha\beta z\, I_m^0 \ll 1$ (valid in our case for $W < 0.5$ mJ)

$$I_m(z) = I_m^0 \exp(-\alpha z) \tag{19}$$

Within the basic reactions 6 and 7, the concentration of the solvated electrons, $N_e(\tau,\xi)$, can be deduced from the following equation

$$\frac{\partial N_e(\tau,\xi)}{\partial \tau} = k_s N_2(\tau,\xi) = \kappa\sigma_a I(\tau,\xi) N_1(\tau,\xi) = \kappa\sigma_a I_m^0 \exp(-\alpha\xi)\exp\left[-\frac{\tau}{\tau_p}\right]^2 (N_1)_0 \exp[-\beta I_m^0 \exp(-\alpha\xi)] \tag{20}$$

For $\beta I_m{}^0 \ll 1$ we obtain

$$N_e(z) = \beta I_m^0 (N_1)_0 [\exp(-\alpha z) - \beta I_m^0 \exp(-2\alpha z)] \tag{21}$$

Equation 2 can be expressed in a differential form ($dA = b\, dz$, cf., Figure 1b)

$$d[\Delta i_p^0(z)] = e_0 E_0 (\mu_e - \mu_-) N_e(z) b dz \tag{22}$$

where b is the fixed width of the electrode in the direction perpendicular to z. Integration from z_0 to $z_0 + L$ and substitution of $N_e(z)$ (eq 21) gives

$$\frac{\Delta i_p^0}{i_d} = \left(\frac{A}{A_{eff}}\right)\left[\frac{\mu_e - \mu_-}{\mu_+ + \mu_-}\right]\kappa\sigma_a\Phi_0\left\{\exp(-\alpha z_0)\left[\frac{1-\exp(-\alpha L)}{\alpha L}\right] - \beta I_m^0 \exp(-2\alpha z_0)\left[\frac{1-\exp(-2\alpha L)}{2\alpha L}\right]\right\} \tag{23}$$

For low-intensity pulses ($W < 0.5-1.0$ mJ at different wavelengths) the second term in eq 23 can be neglected. Thus, the initial linear part of the experimental plots in Figure 2 can be interpreted via the simplified expression

$$\frac{\Delta i_p^0}{i_d} = \gamma_e \gamma_L \sigma_{pd} \Phi_0 \tag{24}$$

where γ_e ($= (A/A_{eff})[(\mu_e - \mu_-)/(\mu_+ + \mu_-)]$) is the constant accounting for the electrochemical properties of the solution and γ_L ($= \exp(-\alpha z_0)[1 - \exp(-\alpha L)]/\alpha L$) is the factor taking into account the gradient of the light intensity via the geometry of the sample.

It is important to emphasize that the interpretation of the experiments by eq 24 is valid only for light pulses of low energy. The nonlinear photodetachment, observed in our experiments at $W > 1$ mJ (Figure 2), has no analytical derivation within the present approximations, thus, requiring a numerical solution of eqs 6−8. On the other hand, it is noteworthy that the simple expression

$$\frac{\Delta i_p^0}{i_d} = \gamma_e[1 - \exp(-\sigma_{pd}\Phi_0)] \tag{25}$$

describing a saturation effect, can be easily obtained for CW light absorption. For transparent solutions (low absorption cross sections and low concentrations) such simplified approach was shown to be satisfactory.[26−28] Nevertheless, employing eq 25 in the pulse experiments may result in false values of cross section and mobilities.

Summarizing this part, we emphasize that the main objective of the above theoretical considerations was to justify the expressions used for the analysis of the experimental data in the nanosecond time scale and to determine the limits of their application.

5. Mechanisms of Electron Photodetachment in Rb/THF. The experimental data on photodetachment cross sections (σ_{pd}) obtained for different excitation wavelengths are presented in Table 1 and Figure 3 (diamonds). Values of σ_{pd} were calculated according to eq 24 and were based on the initial linear plots of $\Delta i_p^0/i_d$ versus Φ_0 (cf. Figure 2 and eq 24) and the parameters γ_e and γ_L. The Rb^- concentrations obtained from the dark current measurements (Figure 1c and eq 3) and the values of σ_a (Figure 3, solid line) were utilized to determine γ_L.

It is noteworthy that the wavelength dependence of the photodetachment cross section qualitatively retraces that of the absorption cross section but with different absolute values (cf. Figure 3). On the other hand, it is obvious that there is a noticeable dependence of the quantum yield, κ, on the photon energy, E_p (cf. Figure 4). The value of κ ($= \kappa_l \approx 0.03$) is constant for the long wavelengths $\lambda \geq 680$ nm ($E_p \leq 1.8$ eV). For the short wavelengths, $\lambda \leq 510$ nm ($E_p \geq 2.4$ eV), the quantum yield κ ($= \kappa_s \approx 0.085$) is also constant but almost three times larger. The inflection region is located approximately at $E_p = 2.2$ eV, which coincides with the ground-state energy of Rb^- relative to the lower edge of the conduction band of THF ($\Delta E = h\nu_{max}^{CTTS} + B$).

The above experimental results clearly point out that there exist two separate energy regions where different mechanisms of the photodetachment prevail. At photon energy $E_p \leq 1.8$ eV, the photodetachment spectrum follows the bell shape part of the absorption spectrum (Figure 3). This implies, to a high accuracy, that the mechanism of CTTS with a subsequent release of e_s^- (eqs 6 and 7) is valid below the conduction band of Rb/THF solution, implying that $\kappa_l = k_s/(k_s + k_c) \approx 0.03$ and, consequently, $k_c = 30k_s$. Thus, the radiationless interconversion is much faster than the solvated electron formation. This observation is in line with the results obtained recently for halide solutions[10,13] and Na/THF system.[21]

The other energy domain is the region where the photon energy obeys $E_p > 2.4$ eV, that is, above the energy gap between the CTTS ground state of Rb^- and the edge of the THF conduction band (Figures 4 and 5b). Under these conditions, direct and autoionization photoinduced transitions into the continuum with generation of quasi-free electrons are feasible. At photon energies slightly below ΔE (inflection region in Figure 4), the transitions into the Anderson's localized states (cf. Figure 5b) are also possible. Thus, within the framework of the energy scheme shown in Figure 5b, at $\lambda \leq 510$ nm, the photodetachment is mainly due to the direct and autoionization transitions (as in the gas-phase photodetachment)[1−3] and the CTTS mechanism can be neglected. This explains the enhancement of κ at shorter wavelengths. Photodetachment via the bound-to-continuum transitions is confirmed by the recent observation of the parabolic wavelength dependence of the magnetic spin relaxation rate of the photoelectrons in photoexcited Rb/THF solutions, which repeats the shape of the electron conduction band (cf. Figure 5b).[24] As a matter of fact, at these wavelengths the parameter κ loses its meaning within

the CTTS model because other mechanisms of photodetachment (not CTTS) are dominant.

Nevertheless, the photodetachment via transitions into the continuum can formally be considered within the framework of eqs 6 and 7 as well. Let us define an energy state (Rb*,e_{qf}) where Rb* is the electronically excited rubidium atom and e_{qf} is the quasi-free electron in the conduction band. This state corresponds to the {Rb ($^2P_{1/2,3/2}$),e^-} energy states, which are responsible for the fine structure thresholds (dips) in the gas-phase photodetachment spectrum of Rb^-.[2] The (Rb*,e_{qf}) state replaces $CTTS_2$ state in eqs 6 and 7 and photoinduced transitions occur between the Rb^- ground state ($CTTS_1$) and this autoionization state. Possessing a very high diffusion coefficient,[69] the quasi-free electron escapes the back recombination (interconversion in terms of the CTTS processes) more efficiently than an electron of the dipole-bound CTTS state. Thus, the electron quantum yield, κ, appears to be higher for autoionization process than for photodetachment via the CTTS state. The electron localization could proceed via an intermediate state (or states) of relatively high energy, lying between the conduction band edge and a solvated electron level. As an example, such presolvated electrons were found to play an important role for releasing an electron from highly excited CTTS states in Cl^-/H_2O system.[10] Thus, an ejected electron loses its energy stepwise from the conduction band via the pre-solvated states, finally approaching the fully solvated state. The origin of the presolvated states may be attributed to "traps" already existing in the liquid due to fluctuations and/or "traps" forming due to local perturbations caused by the Rb^- ion itself. We indicate the overall route from the conduction band to the solvated state by the effective rate constant k_s. It reflects the rate-limiting stage of the above successive processes, found to be in the subpicosecond time scale.[10] The other possibility, namely direct photoinduced transitions from the ground state of Rb^- to the conduction band of the solvent, appears to be ruled out in Rb/THF system. This mechanism should occur with a quantum yield close to unity as shown for O_2^- and CO_2^- in nonpolar solvents.[71−73] Therefore, we believe that it is just autoionization that is mainly responsible for the photodetachment at short wavelengths.

IV. Conclusions

To summarize, we can state that the energy scheme of Figure 5b fully describes the absorption and photodetachment spectra of Rb^- dissolved in THF. We believe that the mechanisms of photodetachment found for Rb/THF in this work are valid also for other alkali-metal/ether solutions and probably for halide aqua systems.[21] Within this context, it might be interesting to examine the electron formation in the two spectral regions shown in Figure 4 by ultrafast optical methods. Time scales of the corresponding kinetics are assumed to be very different, thus, enabling to distinguish between solvated and quasi-free electron species.

Acknowledgment. This work is in partial fulfillment of the requirements for a Ph.D. degree (Y.H.) at the Hebrew University of Jerusalem and was partially supported by a US−Israel BSF grant and by the Volkswagen Foundation (I/73 145). The Farkas Research Center is supported by the Bundesministerium für die Forschung und Technologie and the Minerva Gesellschaft für Forchung GmbH, FRG. The authors thank Prof. B. Schwartz and co-workers for sending us a preprint of their article and Prof. S. Ruhman for useful discussions.

References and Notes

(1) (a) Branscomb, L. M. In *Atomic and Molecular Processes*; Bates, D. R., Ed.; Academic Press: New York, 1962; pp 100−140. (b) Massey, H. *Negative Ions*; Cambridge University Press: Cambridge, 1976.
(2) Frey, P.; Lawen, M.; Breyer, F.; Klar, H.; Hotop, H. *Z. Phys. A: Atoms Nuclei* **1982**, *304*, 155.
(3) Liu, C. N.; Starace, A. F. *Phys. Rev.* **1999**, *A59*, 3643.
(4) Platzman, R.; Franck, L. *Z. Phys.* **1954**, *138*, 411.
(5) Stein, G.; Treinin, A. *Trans. Faraday Soc.* **1959**, *55*, 1086.
(6) Matalon, S.; Golden, S.; Ottolenghi, M. *J. Phys. Chem.* **1969**, *73*, 3098.
(7) Blandamer, M. J.; Fox, M. A. *Chem. Rev.* **1970**, *70*, 59.
(8) Sheu, W. S.; Rossky, P. J. *J. Am. Chem. Soc.* **1993**, *115*, 7729.
(9) Long, F. H.; Shi, X.; Lu, H.; Eisenthal, K. B. *J. Phys. Chem.* **1994**, *98*, 7252.
(10) Gaudual, Y.; Gelabert, H.; Ashokkumor, M. *Chem. Phys.* **1995**, *197*, 167.
(11) Serxner, D.; Dessent, E. H.; Johnson, M. A. *J. Chem. Phys.* **1996**, *105*, 7231.
(12) Sheu, W. S.; Rossky, P. J. *J. Phys. Chem.* **1996**, *100*, 1295.
(13) Kloepfer, J. A.; Vilchiz, V. H.; Lenchenkov, V. A.; Bradforth, S. E. *Chem. Phys. Lett.* **1998**, *298*, 120.
(14) Lehr, L.; Zanni, M. T.; Frischkorn, C.; Weinkauf, R.; Neumark, D. M. *Science* **1999**, *284*, 635.
(15) Collins, G. P. *Scientific American* **1999**, May, 35.
(16) Farkas, A.; Farkas, L. *Trans. Faraday Soc.* **1938**, *34*, 1113.
(17) Salmon, G. A.; Seddon, W. A.; Fletcher, J. W. *Can. J. Chem.* **1974**, *52*, 3259.
(18) Seddon, W. A.; Fletcher, J. W.; Sopchyshyn, F. C.; Selkirk, E. B. *Can. J. Chem.* **1979**, *57*, 1792.
(19) Dye, J. L. *Angew. Chem., Int. Ed. Engl.* **1979**, *18*, 587.
(20) Seddon, W. A.; Fletcher, J. W. *J. Phys. Chem. A* **1980**, *84*, 1104.
(21) Barthel, E. R.; Martini, I. B.; Schwartz, B. J. *J. Chem. Phys.* **2000**, *112*, 9433.
(22) Heimlich, Y.; Rozenshtein, V.; Levanon, H.; Lukin, L. *J. Phys. Chem.* **1999**, *103*, 2917.
(23) Johnson, M. *Science* **1993**, *260*, 320.
(24) Rozenshtein, V.; Heimlich, Y.; Levanon, H. *J. Phys. Chem.* **1997**, *101*, 3197.
(25) Getman, G. D. *DOD/DOE Technology* **1998**, April.
(26) Lukin, L. V.; Balakin, A. A.; Yakovlev, B. S. *Opt. Spectroscopy* **1979**, *47*, 498.
(27) Sowada, U.; Holroyd, R. A. *J. Chem. Phys.* **1980**, *84*, 1150.
(28) Sowada, U.; Holroyd, R. A. *J. Chem. Phys.* **1981**, *85*, 541.
(29) Jou, F. Y.; Dorfman, L. M. *J. Chem. Phys.* **1973**, *58*, 4715.
(30) Dorfman, L. M.; Jou, F. Y.; Wageman, R. *Ber. Bunsen-Ges. Phys. Chem.* **1971**, *75*, 681.
(31) Porter, G. In *Reactivity of the Photoexcited Organic Molecules*; Interscience: London, 1967; pp 79−117.
(32) Calvert, J. G.; Pitts, J. N. *Photochemistry*; Wiley: New York, 1999.
(33) Landau, L. *Physik. Z. Sowietunion* **1933**, *3*, 664.
(34) Marcus, Y. *Ion Solvation*; Wiley: Chichester **1985**.
(35) Formally, the CTTS excited state may be also considered as the Wannier impurity state in an insulator.[36] In other words, the so-called "large polaron" is formed due to a strong electron-medium interaction. It represents autolocalized electron state, that is, a localized phonon cloud coupled to an electron and moved together with it.[37]
(36) Jortner, J.; Gaathon, A. *Can. J. Chem.* **1977**, *55*, 1801.
(37) Lakhno, V. D.; Chuev, G. N. *Physics-Uspekhi* **1995**, *38*, 273.
(38) Radzig, A. A.; Smirnov, B. M. *Reference Data on Atoms, Molecules and Ions*; Springer-Verlag: Berlin, 1985.
(39) Born, M. *Z. Phys.* **1920**, *1*, 45.
(40) Schmidt, W. F. In *Excess Electrons in Dielectric Media*; Ferradini, C., Jay-Gerin, Eds; CRC Press: Boca Raton, 1992; pp 127−159.
(41) Slater, J. C. *J. Chem. Phys.* **1964**, *41*, 3199.
(42) Krestov, G. A. *Thermodynamics of Solvation*, Ellis Horwood Series in Phys. Chem.; Kemp, T. J., Ed.; Ellis Horwood: New York, 1991.
(43) Delahay, P.; Chartier, P.; Nemec, L. *J. Chem. Phys.* **1970**, *53*, 3126.
(44) Mott, N. F. *Conduction in Noncrystalline Materials*; Clarendon Press: London, 1993.
(45) Anderson, P. W. *Phys. Rev.* **1958**, *109*, 1492.
(46) Jou, F. Y.; Freeman, G. R. *J. Phys. Chem.* **1979**, *83*, 2383.
(47) Assel, M.; Laenen, R.; Laubereau, A. *J. Phys. Chem. A* **1998**, *102*, 2256.
(48) Baltuska, A.; Emde, M. F.; Pshenichnikov, M. S.; Wiersma, D. A. *J. Phys. Chem.* **1999**, *103*, 10 065.
(49) Schnitker, J.; Motakabbir, K.; Rossky, P. J.; Friesner, R. *Phys. Rev. Lett.* **1998**, *60*, 456.
(50) Berne, B. J.; Thirumalai, D. *Annu. Rev. Phys. Chem.* **1986**, *37*, 401.
(51) Rossky, R. J.; Schnitker, J. *J. Phys. Chem.* **1988**, *92*, 4277.

(52) Siegman, A. E. *Lasers*; University Science Books: Mill Valley, California, 1986.
(53) Gerischer, H. Z. *Z. Physik. Chem. N. F.* **1960**, *26*, 223 and 325.
(54) Jortner, J.; Ottolenghi, M.; Stein, G. *J. Phys. Chem.* **1964**, *68*, 247.
(55) Morrison, S. R. *Electrochemistry of Semiconductor and Oxidized Metal Electrodes*; Plenum Press: New York, 1980.
(56) Coe, J. V.; Lee, G. H.; Eaton, J. G.; Arnold, S. T.; Sarkas, H. W.; Bowen, K. H. *J. Chem. Phys.* **1990**, *92*, 3980.
(57) Rips, I.; Tachiya, M. *J. Chem. Phys.* **1997**, *107*, 3924.
(58) Chuev, G. N. *Physics-Uspekhi* **1999**, *42*, 149.
(59) For calculations of E_a, we used eqs 2.1, 2.6−2.8, and 2.13−2.17 in ref 57.
(60) Kimura, Y.; Alfano, J. C.; Walhout, P. K.; Barbara, P. F. *J. Phys. Chem.* **1994**, *98*, 3450.
(61) Schwartz, B. J.; Rossky, P. J. *J. Chem. Phys.* **1994**, *101*, 6902.
(62) Yokoyama, K.; Silva, C.; Son, D. H.; Walhout, P. K.; Barbara, P. F. *J. Phys. Chem. A* **1998**, *102*, 6957.
(63) The electronically nonadiabatic interconversion (∼1 ps) is accompanied by electronically adiabatic processes within the p and s states. The latter are accounted for the system evolution along the Marcus-like solvent reorganization coordinate that includes hindered rotations (librations) and translational solvent motion (∼20 fs), followed by diffusion of molecules out of and into the solvation shell (∼ 200 fs).[60−62]
(64) Rozenshtein, V. B.; Gershenzon, Y.; Nalbandian, A. B. *Magnetic Resonance in Gases*; Academy of Sciences: Erevan, 1987.
(65) Nikogosyan, D. N.; Oraevsky, A. A.; Rupasov, V. I. *Chem. Phys.* **1983**, *77*, 131.
(66) Macomber, J. D. *The Dynamics of Spectroscopic Transitions*; Wiley: New York, 1976.
(67) Adiabatic relaxation occurring via the system evolution along the Marcus-like term ($CTTS_2$)[63] can shift an emission wavelength relative to the wavelength of absorbing photons and, thus, also diminish a probability of the stimulated emission.
(68)

$$\frac{\partial I}{\partial z} + \frac{1}{c}\frac{\partial I}{\partial t} = \frac{\partial I}{\partial \xi}\frac{\partial \xi}{\partial z} + \frac{1}{c}\frac{\partial I}{\partial \xi}\frac{\partial \xi}{\partial t}, \frac{\partial \xi}{\partial z} = 1, \frac{\partial \xi}{\partial t} = 0.$$

(69) For quasi-free electrons a mobility, μ_e, of 100 $cm^2V^{-1}s^{-1}$ is typical.[70] With the Einstein equation, $\mu_e = e_0 D_e/kT$, we estimated diffusion coefficient, D_e, of 1 $cm^2\ s^{-1}$.
(70) Bakale, G.; Beck, G. *J. Chem. Phys.* **1986**, *84*, 5344.
(71) Lukin, L. V.; Yakovlev, B. S. *Chem. Phys. Lett.* **1976**, *42*, 307.
(72) Lukin, L. V.; Yakovlev, B. S. *High Energy Chemistry* **1977**, *11*, 440.
(73) Sowada, U.; Holroyd, R. A. *J. Chem. Phys.* **1979**, *70*, 3586.